ISSN 1023-1935, Russian Journal of Electrochemistry, 2016, Vol. 52, No. 2, pp. 99–105. © Pleiades Publishing, Ltd., 2016.
Published in Russian in Elektrokhimiya, 2016, Vol. 52, No. 2, pp. 115–122.

Electrochemical Deposition of Indium: Nucleation Mode and Diffusional Limitation[1]

G. Rakhymbay[a, b, *], M. K. Nauryzbayev[b], B. D. Burkitbayeva[b], A. M. Argimbaeva[b], R. Jumanova[b], A. P. Kurbatov[b], M. Eyraud[a], P. Knauth[a], and F. Vacandio[a]

[a] *Aix-Marseille University, CNRS, MADIREL UMR 7246, 13397 Marseille cedex 20, France*
[b] *Al-Farabi Kazakh National University, Department of Chemistry and Chemical Technology, 71 al-Faraby Ave., Almaty, Kazakhstan*
** e-mail: gulmirarahymbay@gmail.com*

Received June 16, 2014

Abstract—the electrochemical deposition of indium metal from $InCl_3$ solutions was investigated. Cyclovoltammetric experiments showed that the initial hydrogen evolution reaction, observed together with the metal deposition on Pt surface, is blocked when the surface is covered by In. At large cathodic potentials, the current is diffusion-limited. The scan rate dependence of cyclovoltammograms allowed the determination of the diffusion coefficient of In^{3+} ions, 8.18×10^{-6} cm^2/s, using the Delahay equation. The activation energy of diffusion, determined from the temperature dependence of cyclovoltammograms, is about 0.3 eV (23 kJ/mol). Chrono-amperometric experiments are consistent with the cyclovoltammetry; the In^{3+} diffusion coefficient determined using the Cottrell law is in good agreement with the value determined by the Randles-Ševčik equation. Moreover the use of the nucleation models developed by Scharifker and Hills showed a progressive nucleation mode. Electron microscopy observations and X-ray diffraction patterns confirmed the formation of crystalline indium deposits.

Keywords: indium, discharge-ionization, chloride of indium, diffusion coefficient
DOI: 10.1134/S1023193516020087

INTRODUCTION

The future of mankind relies on the existence of sufficient and possibly renewable energy supply. Photovoltaics are a major renewable energy source and recent developments include thin-film solar cells based on $CuInSe_2$ or $CuInS_2$ [1–5] for which major quantities of indium are required; $CuInSe_2$ thin-films are now essentially prepared by electrodeposition [6–8]. Electrodes for polymer electrolyte membrane fuel cells [9, 10] include indium-tin oxides as catalyst support. Furthermore, the advancement of new branches of science and technology is often linked to the progress in the field of microelectronics, including transparent conducting oxides such as Indium–Tin Oxides ITO, [11–15] or light-emitting diodes (LED) containing indium [16]. Semiconducting materials, including (Ga, In)As or InTe, are another important application of indium; their level and rate of development are largely determined by the synthesis from the high-purity elements.

For all these reasons, indium is considered as a strategic element by the EU, because it is currently applied in several key devices and technologies. Its extensive use, especially in liquid crystal display (LCD) flat screens, and its relative scarceness have considerably increased its price. Faced with threats of exhaustion in 2020, it becomes necessary to develop refining methods. The most promising refining methods of indium are electrochemical [17] and a detailed study of the electrochemical processes at the metal-electrolyte interface allows finding the optimal conditions for the preparation and purification of indium, for which Kazakhstan has large mineral reserves. Some publications, monographs and reviews are devoted to the refining of indium in different electrolytes [18–28], but most of them do not apply all modern electrochemical techniques now available. The importance of the problem and the complexity of the interpretation of the results require an extension of experimental methods to provide additional information on mechanisms and intermediate products of the electrode reactions.

In this work, we investigate the electrodeposition of indium by various electrochemical techniques, including cyclovoltammetry and chrono-amperometry. The electrochemical investigation was complemented by SEM and XRD characterizations made on bulk deposits.

[1] The article is published in the original.

Standard and theoretical potentials of various electrode reactions involving In(III) ions

	Standard potential, V/NHE	Theoretical potential, (Nernst equation) V/Ag–AgCl
$In^{3+}_{(aq)} + e = In^{2+}_{(aq)}$	−0.49	−0.71
$In^{3+}_{(aq)} + 2e = In^{+}_{(aq)}$	−0.44	−0.66
$In^{3+}_{(aq)} + 3e = In_{(m)}$	−0.33 [29]	−0.55

1. EXPERIMENTAL

Indium deposition was studied by voltammetric experiments in a classical three-electrode configuration using a Solartron1287 potentiostat-galvanostat. The working electrode was a Pt foil or pure indium metal for control experiments. A Pt grid was used as counter electrode and a saturated Ag–AgCl as reference electrode. All the potentials are indicated relative to Ag–AgCl (E_{ref} = 0.197 V/NHE). The experiments were done in an aqueous solution of 0.1 M $InCl_3$ (99.99% Alfa Aesar) with 1 M NaCl as supporting electrolyte and HCl was added to reach a pH of almost 1. The experiments were performed varying the temperature, the polarization rates and intervals. Current-voltage dependences were determined at least 3 times and processed by graphical and numerical methods to evaluate the reproducibility of the measurements. The scan rate was 20 mV/s. The working electrode was dipped in a concentrated nitric acid solution and rinsed with distilled water before each measurement. From the voltammetric study, reduction potentials for chrono-amperometric experiments were chosen in order to study the mechanism of nucleation from current transient and then obtain bulk Indium deposits for longer deposition times.

Scanning Electron Microscopy (SEM Philips XL-30 FEG) was used to study the morphology of the indium deposits. X-Ray Diffraction (XRD) experiments (D5000 diffractometer, Cu$K\alpha$ radiation) were performed to analyze the phase composition of the deposited layer.

2. RESULTS AND DISCUSSION

2.1. Cyclovoltammetric Study

2.1.1. Mechanism of indium deposition. Electrochemical behavior of indium was studied by number of researchers. In the works Losev [29, 30], process of anodic dissolution of indium in acidic perchlorate solutions leading to formation of In^+ ions was established and proved, which either enter into chemical reactions in solution or oxidize directly to In^{3+} ions on the electrode. Identification In^+ ions was carried out by experiments with the counter electrode unimpaired to polarization. Results of studying the kinetics of the electrochemical behavior of indium in chloride solutions by impedance method was presented by Kozin L.F. [31]. In electrolysis process during the anodic dissolution of the indium, oxidation of In^+ ions to In^{3+} does not occur on indium electrode. In^{3+} ions are formed during the disproportionation reaction of In^{3+} ions in the bulk of the near-electrode layer.

In order to highlight the deposition mechanism, cyclic voltammograms were recorded on Pt electrodes using indium chloride containing solutions (Fig. 1). The initial and final potentials were 0.2 V. Two different cathodic vertex potentials were selected (respectively −0.6 and −1.6 V), in order to clearly identify the cathodic processes.

The first voltammogram (curve *1*) with a −0.6 V vertex potential shows a weak increase in cathodic current (C1), which begins around −0.35 V, followed by a current plateau indicating a diffusion controlled process. For a more cathodic potential (curve *2*), one can see a second large increase in current (C2) at −0.76 V, followed again by a limiting current plateau at −1.3 V. Finally, a third increase in current is observed starting around −1.4 V (C3). The first limiting current ($j_{l,1}$) is about −12 mA/cm^2 while the second limiting current ($j_{l,2}$) is about −56 mA/cm^2. For the slight incursion in the C1 cathodic domain (curve *1*), the corresponding anodic part of this voltammogram is characterized by the absence of an anodic peak even at high magnification. One oxidation peak (A), which begins at E = −0.7 V is clearly correlated with C2 (on curve *2*), as will be confirmed in Fig. 2. This oxidation peak is due to the oxidation of indium into In^{3+}, with the final zero current indicating a total dissolution of the metallic coating.

Latimer et al. [32] as well as Hepler et al. [33] calculated standard potentials from equilibrium constants and proposed the following values (table). In our case, the theoretical redox potential of In^{3+} in equilibrium with various species (In^{2+}, In^+ or In) can be calculated by the Nernst equation assuming that activities can be identified with concentrations. All calculated potentials are reported in table.

According to the potentials calculated in table, the thermodynamically most favorable reaction at a potential of −0.76 V is the In^{3+} reduction into metallic In. According to Piercy et al. [34], the only ion stable in aqueous solution is the In(III) ion, but other oxidation states such as In^+ and In^{2+} may exist in aqueous solutions at low concentration, even though they are unstable at higher concentrations. Thus, with regard to various theoretical potentials calculated in table, it appears that the reduction mechanism of In^{3+} ions is complex. Without rejecting the possibility of intermediate reactions, we can assume that the cathodic current in C2 is mainly due to the reduction of In^{3+} ions to indium metal. To verify this assumption, the potential decrease was stopped at E = −1.2 V and the metal-

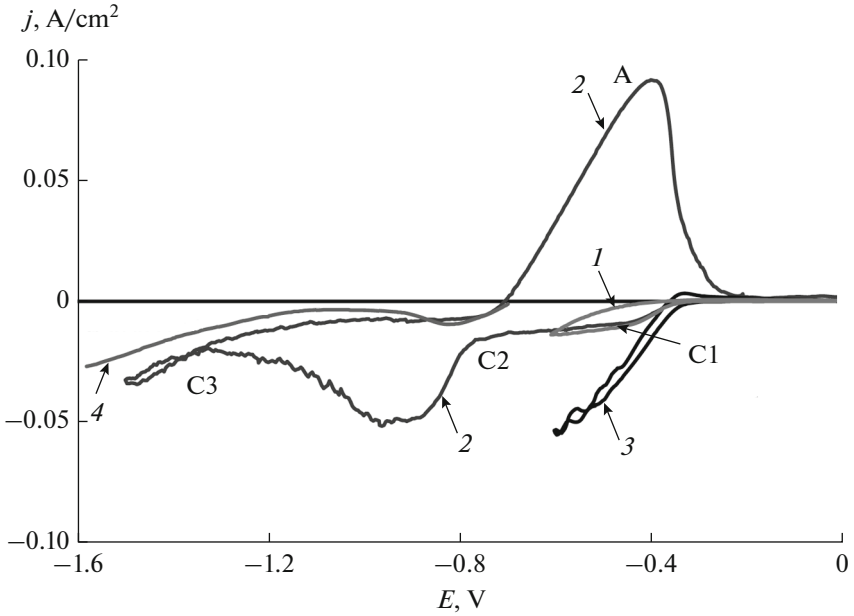

Fig. 1. Voltammograms obtained at 25°C, in a 0.1 M $InCl_3$ + 1 M NaCl solution for platinum for various vertex potentials (*a*) small vertex (*b*), large vertex, and in a 1 M NaCl solution for (*c*) platinum, and (*d*) pure Indium. Scan rate: 20 mV/s.

lographic examination showed the presence of a coating of indium, confirmed by X-ray diffraction.

To attribute C1 and C3 reduction peaks, additional experiments were performed in a blank solution of 1 M NaCl (acidified with HCl to pH 1) on both platinum (curve *3*) and pure indium (curve *4*) electrodes. On voltammogram (*3*), performed in this blank solution, i.e. without In^{3+} ions, one can clearly see an increase of the reduction current at $E = -0.37$ V. This increase of current can be attributed to the reduction of protons, confirmed by the observation of gas bubbles, the Nernst potential ($E = -0.25$ V) and in agreement with the fact that the proton reduction overvoltage on platinum is low. On the anodic part, the small bump is due to the anodic oxidation of hydrogen; H_2 being a gas, the bubbles do not stay on the electrode surface, and the charge associated to this oxidation is significantly lower than for the reduction. One can notice that the reduction of H^+ on Pt occurs in the same cathodic area than C1 from the indium-containing solution. On an indium electrode (curve *4*), the overvoltage for proton reduction is higher and this reduction occurs at about $E = -1.1$ V, in the C3 cathodic zone of the In-containing solution.

These additional experiments allow better understanding of the reduction mechanism. In a first stage, proton reduction occurs on platinum electrodes (C1), but the In^{3+} cations are also attracted by the negative electrode, probably adsorbed on the surface, blocking the reduction of protons, and leading to a current density plateau. At potentials below −0.76 V begins the reduction of In^{3+} into metallic indium (C2) and finally, at about −1.4 V, the C3 current increase is again due to the proton reduction that takes place now on the indium surface.

2.1.2. Scan rate effect. Figure 2 presents the effect of the scan rate on voltammograms obtained on a platinum electrode immersed in the 0.1 M $InCl_3$ + 1 M NaCl solution. The maxima in current of C2 and A peaks are clearly proportional to the scan rate. According to the Delahay equation (Eq. (1)), the current density of the reduction peak j_{peak} of In^{3+} into In should be proportional to the square root of the scan rate (v), at room temperature, this equation becomes:

$$j_p = 0.6105(nF)^{3/2}/(RT)^{1/2}D^{1/2}cv^{1/2}, \qquad (1)$$

where c is a concentration of In^{3+} ions, n the number of electrons involved, D the diffusion coefficient of In^{3+} ions, F Faraday's constant (≈96500 C/mol), R the ideal gas constant (8.314 J/(K mol)) and T the absolute temperature.

The dependence of j_{peak} versus $v^{1/2}$ has been plotted in insertion in Fig. 2. The diffusion coefficient of In^{3+} can be deduced from this equation and is equal to 8.18×10^{-6} cm^2/s, which is in agreement with the value obtained by Timmer et al. [35].

2.1.3. Temperature effect. The influence of the temperature on the In^{3+}/In reduction and oxidation was investigated. The voltamograms obtained are presented in Fig. 3. At temperatures between 25 and 50°C, the voltamograms have similar shape and the reactions involved can be described as previously. When the temperature increases, the cathodic current peak C2, the limiting current $j_{2,l}$, and the anodic current increase too. The diffusion coefficient of In^{3+} ions was calculated from the Randles–Ševčik equation as

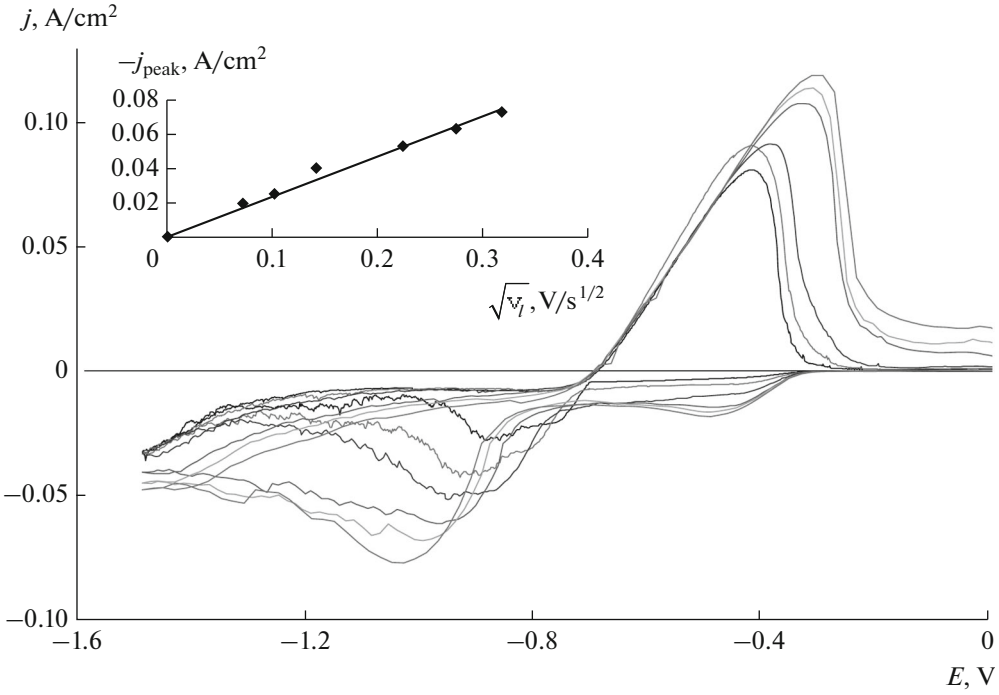

Fig. 2. Voltammograms performed at 25°C on a Pt electrode in a 0.1 M $InCl_3$ + 1 M NaCl solution at various scan rates (5, 10, 20, 50, 75, and 100 mV/s). Inset: evolution of the cathodic j_{peak} C2 versus $\sqrt{v_l}$.

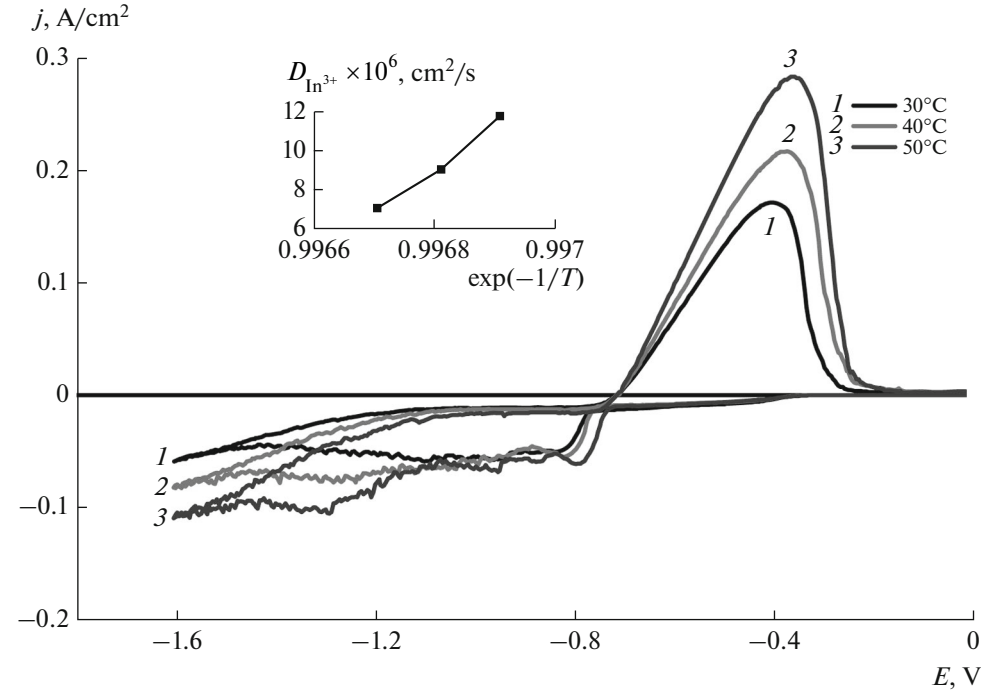

Fig. 3. Voltamograms performed on a Pt electrode in a 0.1 M $InCl_3$ + 1 M NaCl solution at various temperatures. Inset: evolution of $D(In^{3+})$ versus $\exp(-1/T)$.

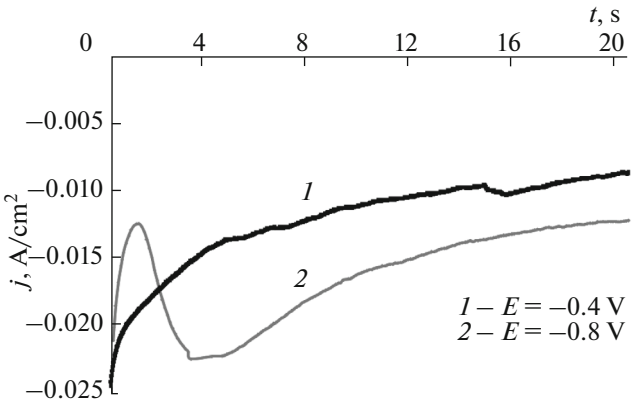

Fig. 4. Current transients obtained at 25°C for the electrodeposition of indium on a Pt electrode in a 0.1M $InCl_3$ + 1 M NaCl solution

function of the temperature considering the variation of the reduction peak C2 from In^{3+} into In. The diffusion coefficient follows an Arrhenius law as described in Eq. (3). The inset of Fig. 3 shows the evolution of D versus $\exp(-1/T)$ according to Eq. (2).

$$D = D_0 \exp\left(\frac{-E_A}{RT}\right). \quad (2)$$

From the slope, we can deduce an activation energy E_A of 23 kJ/mol.

2.2. Chrono-Amperometric Study

2.2.1. Nucleation and growth. The mechanism of nucleation of Indium can be investigated using the chrono-amperometric method. The theoretical models of nucleation have been developed by Scharifker and Hills [36]: they allow distinguishing nucleation and growth modes. The current transients obtained for applied potentials of −0.4 and −0.8 V/Ag–AgCl are presented in Fig. 4.

—At −0.4 V, the monotonous decrease in the cathodic current shows that no nucleation is involved and confirms that this reaction corresponds to hydrogen evolution. The steady-state value of the current is in good accordance with the limiting current determined in Fig. 1.

—At −0.8 V, the cathodic current increases quickly as the area of crystallites increases or new nuclei are formed. After having reached a maximum for j_{max} = −0.06 A/cm² and t_{max} = 3.9 s, the cathodic current decreases towards the limiting current similar to that determined by voltammetry (see Subsection 2.1.1).

In the Scharifker and Hills theory [36], the mass transport process for forming and growing nuclei is achieved by spherical rather than by unidimensional (linear) diffusion. This case is commonly known as 3D nucleation with diffusion-controlled growth. Two types of nucleation mechanisms can be distinguished: instantaneous or progressive nucleation. In instantaneous nucleation, the current will follow the law:

$$\left(\frac{j}{j_m}\right)^2 = \frac{1.9542}{t/t_x}\left\{1 - \exp\left[-1.2564\left(\frac{t}{t_m}\right)\right]\right\}^2 \quad (3)$$

while a progressive nucleation should be described by the relation:

$$\left(\frac{j}{j_m}\right)^2 = \frac{1.2554}{t/t_m}\left\{1 - \exp\left[-2.3367\left(\frac{t}{t_m}\right)^2\right]\right\}^2. \quad (4)$$

From the current transient shown in Fig. 4, $(j/j_m)^2$ is plotted versus (t/t_m) for experimental data as well as for data calculated from both previous theoretical equations. The curves obtained are reported on Fig. 5:

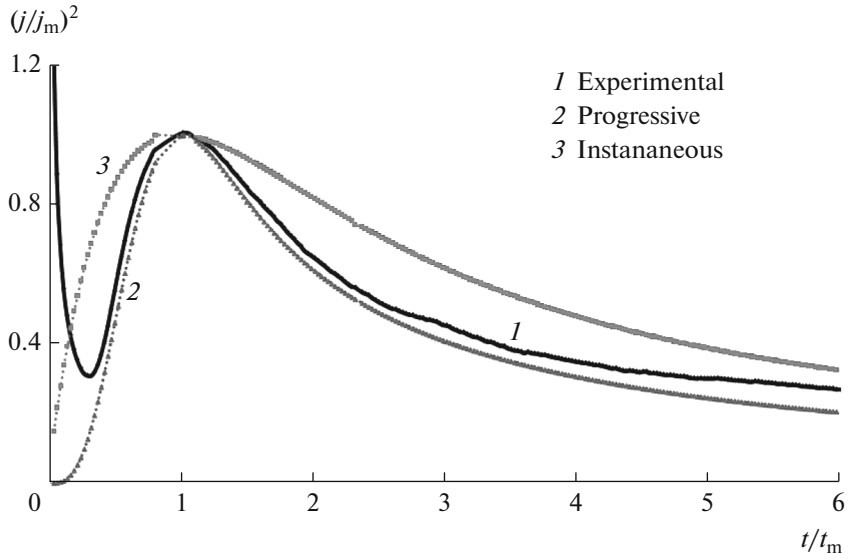

Fig. 5. Comparison between the theoretical models of 3D nucleation with diffusion control growth and the experiment (black line).

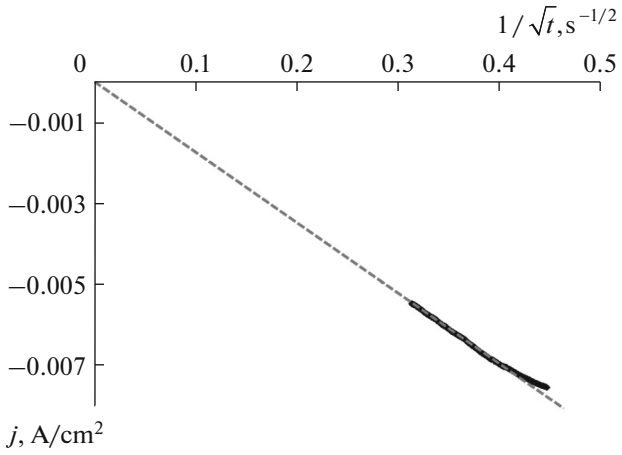

Fig. 6. Cottrel plot used for the determination of the diffusion coefficient of In^{3+}.

the experimental data fit with Eq. (4), showing that the nucleation of Indium is progressive. So the number of crystallites increases with time and variable crystallite sizes are obtained.

In Fig. 6, the variation of current density is plotted as function of the inverse of the square root of time. Cottrell law (Eq. (5)) is satisfied in the linear part of the curve.

$$i = -nF\sqrt{D}\frac{c}{\sqrt{\pi t}}. \quad (5)$$

The diffusion coefficient calculated from the slope of the straight line has a value of 5×10^{-6} cm^2/s, in excellent agreement with the one obtained from the Delahay equation.

2.2.2. Characterization of indium coatings. To verify that the C1 peak evidenced by the voltametric study does not correspond to any indium deposition, a polarization was made during 1 h at –0.6 V. SEM and XRD analysis made on this sample showed that effectively no deposit was observed.

A thick indium coating was deposited at 25°C, onto platinum under potentiostatic condition at a potential of –0.8 V during 20 min. This potential was chosen in order to diminish the diffusion limitation of the reduction. The integration of the curve j–t gives a charge value of –34.1 C/cm^2. Considering the voltammetric study, one can assume that all the current density can be attributed to the In^{3+} ion reduction into metallic indium. In this way, one can deduce a thickness of the coating of about 18 μm according to the Faraday law.

Scanning electronic microscopy was used to characterize the morphology of this coating. The micrographs obtained are presented on Fig. 7 at various magnitudes. The surface of the electrode is covered by a uniform indium layer with an average grain size of about 6.4 μm. The chemical analysis by EDX (in inset of Fig. 7) confirmed the presence of pure indium.

X-ray diffraction experiments were carried out on the same deposit and the diffractogram in θ–2θ coupling mode is presented in Fig. 8. Among the 9 peaks present, 6 peaks are attributable to the indium coating (J.C.P.D.S file no. 005-642), with a body-centered tetragonal structure. The more intense peak is located at 2θ = 33° and corresponds to the (101) plane. Four other less intense peaks are located at 2θ = 36.3°, 54.5°, 63.2° and 69.1°, corresponding respectively to (002), (112), (103) and (202) planes. A small shoulder at 39.2° also corresponds to indium ((110) plane). In addition, three intense peaks located at 2θ = 39.8°, 46.2°, and 67.5° are characteristic of the platinum substrate (J.C.P.D.S file no. 004-0802), still observable under the indium layer, indicating a high porosity of the deposit.

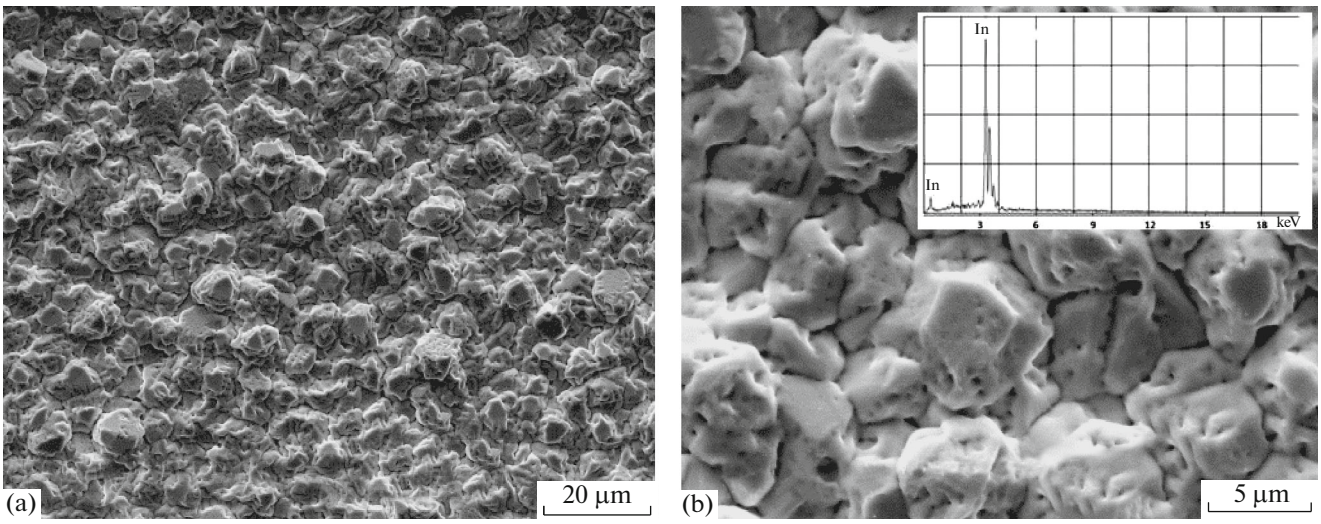

Fig. 7. SEM Images of an indium coating: (a) magnification ×2000, (b) ×8000. Inset: EDX Analysis of Indium coating.

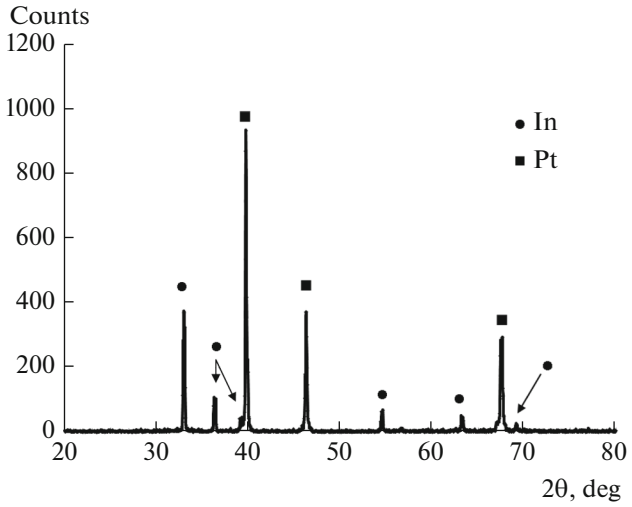

Fig. 8. XRD pattern of Indium coating. (In: J.C.P.D.S file no. 005-642, Pt: J.C.P.D.S file no. 004-0802).

CONCLUSIONS

We studied the electrochemical deposition of indium metal from an $InCl_3$ solution. The indium deposition is preceded by some hydrogen evolution; this reaction is blocked as soon as the Pt electrode is covered by an In layer. In^{3+} reduction is under diffusional control at large cathodic polarization. The diffusion coefficient of In^{3+} can be determined to be $5–6 \times 10^{-6}$ cm^2/s using either the scan rate dependence of cyclovoltammograms (Delahay equation) or chronoamperograms and the Cottrell equation. The activation energy of In^{3+} diffusion is relatively low, 23 kJ/mol. The indium nucleation is progressive, as deduced from the Scharifker and Hills theory.

REFERENCES

1. Goetzberger, A., Hebling, C., and Schock, H.W., *Mater. Sci. Eng., Ser. R*, 2003, vol. 40, p. 1.
2. Panthani, M.G., Akhavan, V., Goodfellow, B., Schmidtke, J.P., Dunn, L., Dodabalapur, A., Barbara, P.F., and Korgel, B.A., *J. Am. Chem. Soc.,* 2008, vol. 130, p. 16770.
3. Lincot, D., *Thin Solid Film*, 2005, vol. 487, p. 40.
4. Cayzac, R., Boulc'h, F., Bendahan, M., Lauque, R., and Knauth, P., *Mater. Sci. Eng., Ser. B,* 2009, vol. 157, p. 66.
5. Cayzac, R., Boulc'h, F., Hornebecq, V., Djenizian, T., Bendahan, M., Pasquinelli, M., and Knauth, P., *J. Mater. Res.,* 2009, vol. 24, p. 3044.
6. Lincot, D., Guillemoles, J.F., Taunier, S., Guimard D., et al., *Solar Energy*, 2004, vol. 77, p. 725.
7. Duchatelet, A., Savidand, G., Vannier, R.N., and Lincot, D., *Thin Solid Films*, 2013, vol. 545, p. 94.
8. Valdes, M., Mollar, M., Vazquez, M., and Mari, B., *J. Appl. Electrochem.*, 2013, vol. 43, p. 619.
9. Chhina, H., Campbell, S., and Kesler, O., *J. Power Sources*, 2006, vol. 161, p. 893.
10. Sharma, S. and Pollet, B.G., 2012, vol. 208, p. 96.
11. Granqvist, C.G. and Hultaker, A., *Thin Solid films*, 2002, vol. 411, p. 1.
12. Minami, T., *Thin Solid Films*, 2008, vol. 516, p. 5822.
13. Lupan, O., Guerin, V.M., Tiginyanu, I.M., Ursaki, V.V., Chow, L., Heinrich, H., and Pauporte, T., *J. Electrochem. Photobiology, Ser. A,* 2010, vol. 211, p. 65.
14. Miettunen, K., Halme, J., Vahermaa, P., Saukkonen, T., Toivola, M., and Lund, P., *J. Electrochem. Soc.*, 2009, vol. 156, p. B876.
15. Park, Y.S., Park, H.K., Jeong, J.A., Kim, H.K., Choi, K.H., Na, S.I., and Kim, D.Y., *J. Electrochem. Soc.*, 2009, vol. 156, p. H588.
16. Zhmakin, A.I., *Phys. Rep., Rev. Section Phys. Lett.*, 2011, vol. 498, p. 189.
17. Hee Nam Kang, Jin-Young Lee, and Jong-Young Kim, *Hydrometallurgy*, 2011, vol. 110, p. 120.
18. Zhou Zhi-hua, Mo Hong-bing, and Zeng Dong-ming, *Trans. Nonferrous Met. Soc. China*, 2004, vol. 14, p. 637.
19. Kozin, L.F., Nagibin, S.N., and Chabanenko, Y.I., *High-Purity Substances*, 1996, vol. 5, p. 30.
20. Alfantazi, A.M. and Moskalyk, R.R., *Miner. Eng.*, 2003, vol. 16, p. 687.
21. Gunawardena, G., Pletcher, D., and Razaq, A.J., *J. Electroanal. Chem.,* 1984, vol. 164, p. 363.
22. Walsh, F.C. and Gabe, D.R., *Surf. Technol.*, 1979, vol. 8, p. 87.
23. Walsh, F.C. and Gabe, D.R., *Surf. Technol.*, 1978, vol. 6, p. 425.
24. Canegallo, S., Demeneopoulos, V., Peraldo Bicelli, L., and Serravalle, G., *J. Alloys Compounds*, 1995, vol. 228, p. 23.
25. Chung, Y. and Lee, C.-W, *J. Electrochem. Sci. Technol.*, 2012, vol. 3, p. 1.
26. Munoz, A.G. and Bessone, J.B., *Electrochim. Acta*, 1998, vol. 43, p. 1067.
27. Kozin, V.F. and Omelchuk, A.A., *Metallurgy Rare Precious Met.*, 2006, vol. 2, p. 45.
28. Munoz, A.G. and Bessone, J.B., *Electrochim. Acta*, 1998, vol. 43, p. 2033.
29. Molodov, A.I., Markosyan, G.N., and Losev, V.V., *Electrochemistry*, 1973, vol. 9, p. 1368.
30. Dmitrenko, S.V., Molodov, A.I., and Losev, V.V., *Electrochemistry*, 1984, vol. 20, p. 1159.
31. Kozin, L.F., Sushkov, Ya.P., and Kurdyumova, T.A., *Ukrain. J. Chem.,* 1974, vol. 40, p. 1136.
32. Latimer, W.M., *The Oxidation States of the Elements and their Potentials in Aqueous Solutions*, 2nd Ed., N.Y.: Prentice-Hall, Inc., 1952.
33. Hepler, L.G., Hugus, Z.Z., and Latimer, W.M., *J. Am. Chem. Soc.*, 1953, vol. 75, p. 5652.
34. Piercy, R. and Hampson, N.A., *J. Appl. Electrochem.*, 1975, vol. 5, p. 1.
35. Timmer, B., Sluyters-Rehbach, M., and Sluyters, J.H., *J. Electroanal. Chem.,* 1968, vol. 19, p. 73.
36. Scharifker, B. and Hills, G., *Electrochim. Acta*, 1983, vol. 28, p. 879.